PAM-N signaling by coupling modulation in a ring resonator

Samira Karimelahi* and Ali Sheikholeslami

Department of Electrical and Computer Engineering, University of Toronto, 10 King's College Road, Toronto, Ontario M5S 3G4, Canada

**Corresponding author: samira@ece.utoronto.ca*

Received October 2, 2014; accepted November 19, 2014;
posted December 16, 2014 (Doc. ID 224294); published January 22, 2015

A new method for an all-optical PAM modulation is presented. The method relies on coupling modulation of a ring resonator with an RF length much shorter than the previously proposed segmented MZI. The PAM modulator is optimized in terms of linearity both for the reverse and forward-biased cases. This modulator can operate for long haul communication with data rate only limited by the bandwidth of the MZI. © 2015 Optical Society of America

OCIS codes: (230.4110) Modulators; (230.5750) Resonators; (060.4510) Optical communications; (230.1150) All-optical devices.

http://dx.doi.org/10.1364/OL.40.000332

To address the increasing demand for higher data rates, it is essential to increase the spectral efficiency of optical transmission systems by moving from on–off keying (OOK) to more advanced modulation formats. One of the prime modulation candidates is pulse amplitude modulation (PAM) where data is represented by different levels of signal amplitude with the possible advantage of direct detection. Multilevel optical intensity was achieved using electrical digital-to-analog converters (DAC) to either drive vertical-cavity surface-emitting lasers (VCSEL) [1] or Mach–Zehnder interferometers (MZI) [2]. However, in addition to the imposed chirp in the directly modulated laser (DML), the design of a linear DAC operating at high frequencies could be challenging [3]. An all-optical DAC was realized by segmented MZI in CMOS process where the total length of the phase shifter was decreased from a few mm in a conventional lateral pn junction to about 500 μm in a silicon-insulator–silicon-capacitor (SISCAP) [4]. Although this is a considerable progress in terms of reducing the device footprint, we propose a solution to further reduce this footprint.

Inspired by the paper by Yariv [5] and follow-up works by Sacher and co-workers [6–8], we propose an all-optical optical PAM implementation by adding feedback to the segmented MZI. Having feedback in the optical path requires a much shorter RF length compared to the segmented MZI in [4] using either SISCAP or the conventional lateral pn/pin junction. Similar to [4], use of the small phase shifters leads to lower power consumption in electrical drivers as there will be no need to drive power-hungry transmission line terminations. Moreover, similar to conventional MZI, push–pull driven MZI-assisted ring can operate for long-haul communication purposes as it does not cause chirp [6,9].

The proposed device schematic for PAM-4 signaling using MZI-assisted ring is shown in Fig. 1. For simplicity, a PAM-4 configuration is illustrated here, while the same concept can be extended to PAM-N by using $\log_2(N)$ pn/pin phase shifter segments.

Optical power transmission can be modulated from theoretical 0 to unity by varying the phase difference in the MZI arms, $\Delta\phi$, between $2\sin^{-1}(\alpha)$ and π for the direct connected feedback MZI-assisted ring with the ring transmissivity of α [5]. For the case of $\alpha = 0.99$, the required $\Delta\phi$ is around $\frac{\pi}{11}$, which leads to a much smaller required RF length and drive voltage compared to the conventional MZI.

By segmenting the length of the pn/pin phase shifter, L, into L_1 and L_2, where $L = L_1 + L_2$ and $L_2 > L_1$ (e.g., $L_2 = 2L_1$), multilevel optical modulation can be achieved. The segments with length of L_1 and L_2 can be treated as lumped circuit elements without any requirement for transmission line driver. Assuming a loss-less MZI, the through and cross-coupling coefficients (t and κ) from input port (A) in Fig. 1 to the output port (B) and to the ring (C), respectively, are:

$$t = -i\,\sin\left(\frac{\phi_0 + \Delta\phi'(t)}{2}\right)$$
$$\kappa = i\,\cos\left(\frac{\phi_0 + \Delta\phi'(t)}{2}\right). \quad (1)$$

Here ϕ_0 is the DC operating phase (that can be induced by the thermal tuner in Fig. 1 or by a length difference between the two arms), and $\Delta\phi'(t) = \Delta\phi'_{L1}(t) + \Delta\phi'_{L2}(t)$ where $\Delta\phi'_{L1}(t)$ and $\Delta\phi'_{L2}(t)$ are the time-varying phase accumulation difference between the two arms of the first and second pn/pin phase shifter segments, respectively. In the case where both segments are driven in push–pull scheme, $\phi'_1(t) = -\phi'_2(t) = \frac{\Delta\phi'(t)}{2}$ where $\phi'_1(t)$ and $\phi'_2(t)$ are the time-dependent phase accumulation of the first and second arms.

A summary of the device operation principle is shown in Table 1 for push–pull drive where L_1 and L_2 represent the segments with length of L_1 and L_2, respectively.

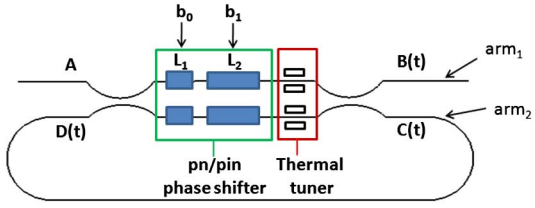

Fig. 1. Schematic of the proposed PAM-4 modulator using the MZI-assisted ring.

The first column shows the bit sequence for 2 bits/symbol in PAM-4 case. The next four columns illustrate the RF drive voltage for segments in each MZI arm, and the last column shows the corresponding phase difference between MZI arms. L_1 represents the least significant bit, while L_2 corresponds to the most significant bit.

By substituting t from Eq. (1) into the power transmission from [10], the following can be derived in the steady state for MZI-assisted ring:

$$\frac{P_{\text{out}}}{P_{\text{in}}} = \frac{\alpha^2 - 2\alpha\left|-i\sin\left(\frac{\phi_0+\Delta\phi'}{2}\right)\right|\cos\theta + \left|-i\sin\left(\frac{\phi_0+\Delta\phi'}{2}\right)\right|^2}{1 - 2\alpha\left|-i\sin\left(\frac{\phi_0+\Delta\phi'}{2}\right)\right|\cos\theta + \left|-i\sin\left(\frac{\phi_0+\Delta\phi'}{2}\right)\right|^2\alpha^2} \tag{2}$$

where θ includes feedback phase shift plus the phase shift through the coupler, and $\Delta\phi'$ takes any of the 4 values presented in Table 1. The static on-resonance transmission which occurs when $\theta = 2m\pi$, m an integer, is:

$$\left(\frac{P_{\text{out}}}{P_{\text{in}}}\right)_{\text{res}} = \frac{\left(\alpha - \left|-i\sin\left(\frac{\phi_0+\Delta\phi'}{2}\right)\right|\right)^2}{\left(1 - \alpha\left|-i\sin\left(\frac{\phi_0+\Delta\phi'}{2}\right)\right|\right)^2}. \tag{3}$$

The performance of the modulator on resonance strongly depends on α where lower loss in the feedback leads to lower required modulation in the coupling coefficient.

L_1 and L_2 can be selected based on binary weighting or other schemes such as thermometer weighting where $(N-1)$ pn segments for PAM-N implementation are needed [4]. Here we follow the binary-weighted scheme where $L_2 = 2L_1$, which leads to linear phase steps with respect to ϕ_0. This assumption will be revisited later in the paper.

The proposed modulator is electro-optically simulated to study the performance. A device simulator from Lumerical Solution Inc. [11] is used with lateral pn junction parameters provided by Institute of Microelectronics (IME)/A*STAR [12]. The wavelength-dependent effective index is determined using a commercial mode solver. The MZI was considered to be loss-less, and a propagation loss of 2 dB/cm is assumed for the passive waveguides, which corresponds to $\alpha = 0.988$. The total phase shifter length is 340 μm with a loaded Q of 1.86×10^5 at 1.55 μm and a feedback length of 490 μm. The RF voltage for reverse-biased pn junction is taken to be $2V_{pp}$. The device is biased at $\phi_0 = 3.01$ rad, which corresponds to the dc phase where the on-resonance transmission in Eq. (3) reaches 0.5.

Table 1. Summary of PAM-4 Operation Principle Using the Proposed Device

	arm_1		arm_2		
b_1b_0	L_2	L_1	L_2	L_1	$\Delta\phi'$
00	$\frac{-V}{2}$	$\frac{-V}{2}$	$\frac{V}{2}$	$\frac{V}{2}$	$\Delta\phi'_1$
01	$\frac{-V}{2}$	$\frac{V}{2}$	$\frac{V}{2}$	$\frac{-V}{2}$	$\Delta\phi'_2$
10	$\frac{V}{2}$	$\frac{-V}{2}$	$\frac{-V}{2}$	$\frac{V}{2}$	$\Delta\phi'_3$
11	$\frac{V}{2}$	$\frac{V}{2}$	$\frac{-V}{2}$	$\frac{-V}{2}$	$\Delta\phi'_4$

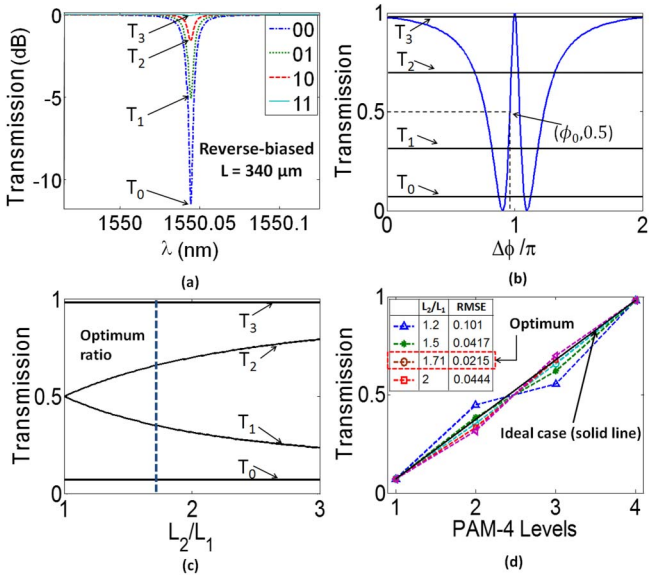

Fig. 2. (a) Sample optical transmission spectra for four symbols in PAM-4 format for binary-weighted scheme. (b) On-resonance transmission versus normalized $\Delta\phi$ for the same device. (c) T_0 to T_3 versus L_2 to L_1 ratio. (d) T_0 to T_3 corresponding to each level in PAM-4 for various ratios of L_2 to L_1. The ideal case for the same device is also plotted as a solid line.

Figure 2(a) plots the transmission spectra for input bit sequences of 00, 01, 10, and 11 according to Eq. (2). An ER of about 11 dB between 00 to 11 is observed. This ER can be increased further by increasing L or peak-to-peak RF applied voltage; however, here, the optical modulation amplitude (OMA) is maximized to maximize the eye opening.

The on-resonance transmission versus normalized $\Delta\phi$ given by Eq. (3) is shown in Fig. 2(b). The biased phase (ϕ_0), located in the most linear part of the transfer function, is also indicated in the figure. The modulator is biased at an under-coupled condition where $|t|$ at ϕ_0 is greater than α. Also shown are the values of the power transmission at the resonance wavelength, indicated as T_0, T_1, T_2, and T_3. As illustrated in Fig. 2(b), despite the linear phase steps in binary-weighted segments, due to the nonlinear nature of the transfer function, the power levels are not distributed uniformly, which may pose challenges for higher-order PAM signaling.

To distribute the power levels more linearly, the ratio of L_2 to L_1 needs to be optimized. Figure 2(c) shows how the power transmission of each level varies as a function of L_2/L_1 for the aforementioned parameters of the reverse-biased MZI-assisted ring modulator. Note that T_0 and T_3 stay constant independent of the ratio because L is constant, while T_1 and T_2 change in the opposite directions. Also, according to Fig. 2(c), for the case where $L_2 = L_1$, the number of output levels decreases from 4 to 3 as $T_1 = T_2$. The optimum ratio was found based on the minimum root-mean-square error (RMSE) with respect to the line connecting T_0 to T_3 shown in solid black line in Fig. 2(d). Also plotted are T_1 and T_2 for a few selected L_2 to L_1 ratios including the optimum ratio of 1.71 marked by the red dotted box in the inset of Fig. 2(d).

The corresponding RMSE for each case is also indicated in the inset of the figure. Note that the optimized L_2 to L_1 ratio may differ in the transient case as the power levels are slightly different, and device response is affected by memory-effect distortion [9]. Nevertheless, the same method can be applied to find the optimum ratio in the transient case.

In some applications where a higher linearity is desirable for power level distribution, the number of segments can be optimized as well as their lengths. On the other hand, in an optical link with dominant shot noise whose variance rises with square root of input power [13], nonuniform power levels may be favorable to meet the desired BER for each level. Also, binary-weighted segments might provide desirable power level distribution depending on the SNR requirements in the optical links.

To decrease the length of the phase shifter further, one can use forward-biased p-i-n junction and take advantage of a much higher refractive index change as a function of the applied voltage (around 8×10^{-4} for 0 to 1 V). In this case, L can be decreased by about 19× compared to the reverse-biased condition not only due to the stronger electro-optic effect but also due to the smaller required feedback length and as a result a higher α. The transmission spectra and the on-resonance transmissions are shown in Figs. 3(a) and 3(b), respectively. The optimum ratio of L_2 to L_1 is calculated to be around 1.68. The result of the segment length optimization is more clear when comparing almost equally spaced power levels in Fig. 2(b) with binary-weighted case in Fig. 3(b). The RF length for forward-biased case is about 27× smaller than what has been reported in [4] for segmented MZI in a SISCAP process with the same applied voltage. Using pre-emphasis scheme to drive the device overcomes the modulation speed limitations of the forward-biased diode [14], but it may add to the complexity of the driver circuit limiting the achievable operation speed [15].

It has been shown that MZI-assisted rings, used for OOK modulation, do not impose any optical bandwidth limitations other than the cavity FSR, and the upper limit for modulation speed is determined by the MZI bandwidth [9]. In order to verify the low-distortion PAM-4 modulation in the non-quasi-static mode of operation in the cavity, transient simulations are performed. The cavity response to a return to zero (RZ) PAM-4 driving phase is simulated based on the following equations [9]:

$$
\begin{aligned}
B(t) &= t(t)A + \kappa(t)D(t) \\
C(t) &= -\kappa^*(t)A + t^*(t)D(t) \\
D(t) &= \alpha e^{-i\theta_{fb}} C(t-\tau),
\end{aligned} \tag{4}
$$

where A is the amplitude of a continues-wave input, and B, C, D are the time-dependent slow-varying envelopes of the electric field at the locations shown in Fig. 1. Propagation time and phase shift in the feedback are τ and θ_{fb}, respectively.

The modulator is considered to have a feedback length of 220 μm and a waveguide loss of 2 dB/cm corresponding to $\alpha = 0.995$. Loaded Q is 1.86×10^5 for 1550 nm wavelength with about 1 GHz cavity linewidth. The effective refractive index at 1550 nm is used, and τ is about 3 ps. FSR is greater than 300 GHz. An RZ-PAM-4 random Gaussian signal with a period of 20 ps and a pulse duration of 7 ps (FWHM), shown in Fig. 4(a), is used to drive the device on the resonance frequency. In Fig. 4(a), the maximum and minimum values of the phase modulation are optimized to have a maximum OMA between T_0 and T_3, and the middle values of the phase modulation are selected according to the optimum L_2 to L_1 ratio for linearity of the output power levels in the transient mode. The modulation frequency corresponds to the maximum achieved data rate with MZI [16] in depletion mode and is well above the cavity linewidth of 1 GHz to study the non-quasi-static mode. However, for a more accurate estimation of upper speed limit, the electrical constraints such as RC time constant of the MZI pn junction and wiring should be taken into account.

The device is modulated after being operated in the steady state for a few cycles. The eye diagram which corresponds to the aforementioned RZ input sequence is shown in Fig. 4(b). Despite the memory effect distortion present in the under-coupled MZI-assisted ring modulator [9], the eye is completely open for non-quasi-static mode of 50-Gsymbols/s (100 Gb/s). Four transmission levels can be observed in the eye diagram. As the modulator is on resonance, only a small variation of about 0.15 rad in $\Delta\phi$ is required to induce a large difference of 0.76 between the highest and the lowest output

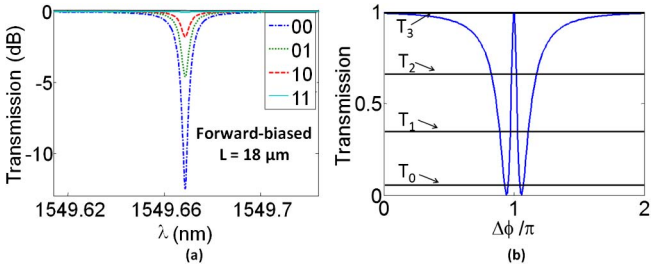

Fig. 3. (a) Sample optical transmission spectra for four symbols in PAM-4 format with optimized L_2 to L_1 ratio. (b) On-resonance transmission versus normalized $\Delta\phi$ for the same device.

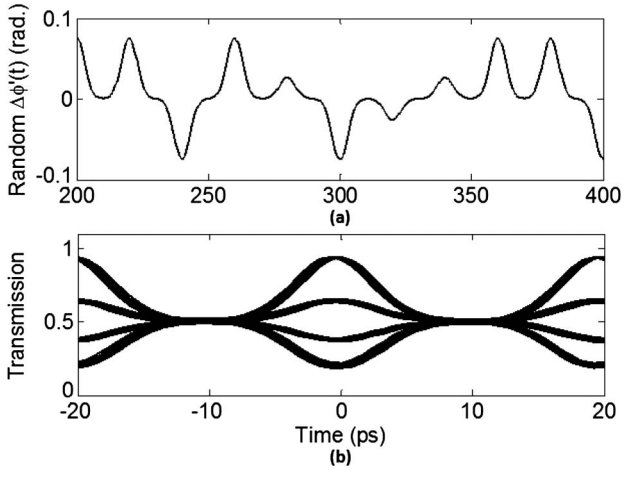

Fig. 4. (a) Push–pull RZ PAM-4 random input sequence of $\Delta\phi'(t)$. (b) RZ PAM-4 eye diagram for the random sequence shown in (a), for optimized L_2 to L_1 ratio.

transmission levels. This leads to a much smaller required drive voltage compared with MZI, which requires π phase shift.

To summarize, we have proposed a device to facilitate PAM-N modulation format using an all-optical DAC that requires shorter RF length and lower voltage compared with the segmented MZI. The proposed configuration can be designed to work under reverse or forward bias. Reverse-biased case is a better candidate for high-speed modulation but requires higher than $1V_{pp}$, which makes it challenging for integration with sub-1 V CMOS technology. The forward-biased case is a better candidate for low-speed operation as it can be driven by less than $1V_{pp}$, which makes it feasible for integration with advanced CMOS circuits.

The authors are grateful for the financial support of the Natural Sciences and Engineering Research Council of Canada.

References

1. J. E. Cunningham, D. Beckman, X. Zheng, D. Huang, T. Sze, and A. V. Krishnamoorthy, Opt. Express **14**, 12028 (2006).
2. M. Nakazawa, S. Okamoto, T. Omiya, K. Kasai, and M. Yoshida, in *Optical Fibers and Communications Conference* (2010), paper OMJ5.
3. K. Doris, J. Briaire, D. Leenaerts, M. Vertregt, and A. Van Roermund, IEEE ISSCC **1**, 116 (2005).
4. X. Wu, B. Dama, P. Gothoskar, P. Metz, K. Shastri, S. Sunder, J. Van der Spiegel, Y. Wang, M. Webster, and W. Wilson, in *IEEE International Solid-State Circuits Conference Digest of Technical Papers (ISSCC)* (IEEE, 2013), pp. 128–129.
5. A. Yariv, IEEE Photon. Technol. Lett. **14**, 483 (2002).
6. W. D. Sacher, W. Green, S. Assefa, T. Barwicz, H. Pan, S. Shank, Y. Vlasov, and J. Poon, Opt. Express **21**, 9722 (2013).
7. W. D. Sacher, W. M. J. Green, D. M. Gill, S. Assefa, T. Barwicz, M. Khater, E. Kiewra, C. Reinholm, S. M. Shank, Y. A. Vlasov, and J. K. S. Poon, Opt. Express **22**, 20252 (2014).
8. W. D. Sacher and J. K. Poon, Opt. Lett. **34**, 3878 (2009).
9. W. D. Sacher and J. K. S. Poon, J. Lightwave Technol. **27**, 3800 (2009).
10. A. Yariv, Electron. Lett. **36**, 321 (2000).
11. https://www.lumerical.com.
12. http://www.ime.a-star.edu.sg/PPSSite/index.asp.
13. J. R. Janesick, Proc. SPIE **170**, 22 (2007).
14. Q. Xu, S. Manipatruni, B. Schmidt, J. Shakya, and M. Lipson, Opt. Express **15**, 430 (2007).
15. C. Li, R. Bai, A. Shafik, E. Z. Tabasy, G. Tang, C. Ma, C. H. Chen, P. Zhen, M. Fiorentino, P. Chiang, and S. Palermo, in *IEEE International Solid-State Circuits Conference Digest of Technical Papers (ISSCC)* (IEEE, 2013), pp. 124–125.
16. D. J. Thomson, F. Y. Gardes, J. M. Fedeli, S. Zlatanovic, Y. Hu, B. P.-P. Kuo, E. Myslivets, N. Alic, S. Radic, G. Z. Mashanovich, and G. T. Reed, IEEE Photon. Technol. Lett. **24**, 234 (2012).